Absorption and scattering in photo-thermo-refractive glass induced by UV-exposure and thermal development

Julien Lumeau [a,b,*], Larissa Glebova [c], Leonid B. Glebov [a]

[a] CREOL/the College of Optics and Photonics, University of Central Florida, 4000 Central Florida Blvd Orlando, FL 32816-2700, USA
[b] Aix-Marseille Université, CNRS, Centrale Marseille, Institut Fresnel, UMR 7249, 13013 Marseille, France
[c] OptiGrate Corporation, 562 S, Econ Circle, Oviedo, FL 32765, USA

ABSTRACT

Photo-thermo-refractive (PTR) glass is a multicomponent photosensitive silicate glass that, after successive UV-exposure and thermal treatment, exhibits a refractive index change that results from the precipitation of nano-crystalline NaF. This glass is successfully used for the fabrication of holographic optical elements (volume Bragg gratings) that dramatically enhance properties of numerous laser systems and spectrometers. In this paper, induced absorption and scattering that determine efficiency of such elements were studied. It is found that the main contribution to induced absorption is produced by several types of silver containing particles having absorption bands with maxima in the blue-green region with exponential tails extending to the near IR spectral region. Evolution of all absorption bands was studied for different conditions of UV exposure and thermal development. Complex mechanisms of interconversion of silver containing particles is demonstrated as well as the fact that some of these particles can be associated with catalyzers of the nucleation process. It is also found that induced scattering obeys the classic Rayleigh law with an intensity depending on the conditions of UV exposure and thermal development. For short development times, scattering increases with dosage because of increased volume fraction of crystalline phase. For long development times, scattering decreases with dosage because of decreased size of individual crystals.

© 2013 Elsevier B.V. All rights reserved.

1. Introduction

Photo-thermo-refractive (PTR) glass is a photosensitive $Na_2O–NaF–K_2O–KBr–ZnO–Al_2O_3–SiO_2$ glass, doped with minor amounts of Ce, Ag, Sb, and Sn, that undergoes a permanent refractive index change after UV-exposure followed by thermal treatment [1,2]. PTR glass has been used for holographic recording of various types of volume diffractive optical elements [3], and finds a wide range of applications such as spectral beam combining, the selection of transverse and longitudinal modes in laser resonators, beam deflectors, splitters and attenuators [4,5]. A simplified description of the photo-induced reactions in glasses with similar composition can be summarized as:

(i) photoionization of Ce^{3+} and formation of atomic silver during exposure to UV ($Ag^+ + Ce^{3+} + h\nu \rightarrow Ag^0 + Ce^{4+}$),
(ii) silver containing particles clustering during an initial stage of thermal treatment below 500 °C ($nAg^0 + kT \rightarrow Ag_n^0$), and

(iii) heterogeneous nucleation and growth of NaF nanocrystals on further heating at temperatures exceeding 500 °C [6].

It was shown that the refractive index change required for holographic recording is the result of the precipitation of this crystalline phase [7,8]. No other crystalline phases were detected in PTR glass developed at relatively low temperatures normally used for hologram recording [9]. In addition, crystalline NaF does not have any absorption bands in the near-UV, visible and near-IR spectral regions. However, it was demonstrated that an induced absorption band mainly in the blue region and with a complex spectrum evolves in the process of thermal treatment of UV-exposed samples [10]. It was proposed that this band could be associated with silver and bromine-containing particles. However, no further analysis was carried out at that time. In this paper, loss spectra induced in PTR glass after UV-exposure and thermal treatment are analyzed in detail. Photo-induced absorption and scattering were discriminated and then analyzed. Absorption spectra were decomposed into Gaussian functions that could be associated with different types of particles appearing in the glass at different stages of the thermal treatment. Using this model, the evolution of each particle during the nucleation and the thermal development processes were studied. Scattering spectra are also mathematically

* Corresponding author at: Aix-Marseille Université, CNRS, Centrale Marseille, Institut Fresnel, UMR 7249, 13013 Marseille, France. Tel.: +33 672 289 061.
   E-mail address: julien.lumeau@fresnel.fr (J. Lumeau).

analyzed and their evolution was also studied at different stages of the thermal treatment.

2. Experimental

2.1. PTR glass preparation

Samples of a photosensitive PTR glass containing 15Na$_2$O–5ZnO–4Al$_2$O$_3$–70SiO$_2$–5NaF–1KBr–0.01Ag$_2$O–0.01CeO$_2$ (mol.%) and minor amounts of Sn and Sb were used in this work as in previous studies [7,11–13]. The glasses were melted in a platinum crucible, stirred, cooled to the glass transition temperature, and annealed (2 h at 460 °C and cooled down with rate of 0.1º/min). Polished 25 × 25 × 5 mm^3 samples were prepared from the billet. The homogeneity of the PTR glass samples is a critical parameter affecting crystallization properties [14]. Therefore, optical homogeneity of each sample was tested by the shadow method in a divergent beam of a He–Ne laser and quantified by measurements using a Fizeau interferometer (GPI, Zygo Corp.). The samples prepared for this study had refractive index fluctuations of less than 40 ppm (4×10^{-5}), peak-to-valley, across the 25 × 25 mm^2 aperture.

2.2. UV-exposure and heat-treatments

UV-exposure of samples was performed using the beam of a He–Cd laser (power: 4 mW, wavelength: 325 nm, diameter: 1 mm). Samples were homogeneously exposed with a dosage ranging from 0.25 to 8 J/cm^2 by scanning the laser beam to produce multiple overlapped stripes on the sample. Dosage was controlled by changing the scanning speed [15]. The samples were heat-treated at 480 and 515 °C. The samples heat-treated at 480 °C were dropped inside the temperature stabilized furnace and, at the end of each thermal treatment, were quenched in order to control the thermal treatment duration with precision better than 1 min. This method allowed performing short thermal treatments. The samples treated at 515 °C were heated from room temperature at a rate about 20 K/min, aged at 515 °C and then cooled down to room temperature in the furnace following its natural cooling rate about 2.5 K/min. Finally, in order to remove any incipient crystallization on surfaces, each sample was ground and re-polished to a flatness better than $\lambda/2$ at 633 nm.

2.3. Spectral measurements

Spectra of losses (sum of absorption and scattering) were measured using a Perkin Elmer Lambda 950 spectrophotometer in the range from 200 to 1700 nm. Optical density $OD = \log_{10}(1/T)$, where T is transmission, was used for all calculations. Internal optical density (OD_i) was routinely calculated by subtraction of Fresnel reflection (OD_r) that was determined from a dispersion curve of PTR glass: $OD_i = OD - OD_r$. Losses coefficient was calculated as L, cm^{-1} = $A + S = OD_i/t$, where A and S are coefficients of absorption and scattering and t is the sample's thickness in centimeters. Photometric absolute accuracy of the Perkin Elmer Lambda 950 was about $\Delta OD = \pm 0.005$ and fluctuations of Fresnel reflection related to the specific condition of the surfaces could attain $\Delta OD_r = \pm 0.005$ resulting in the absolute precision of our spectrophotometric measurement for 0.5-cm-thick samples of about 2×10^{-2} cm^{-1}. To achieve higher precision of measurements, both the transmission and the reflection at 1085 nm were carried out by a precise photometer based on an Yb-doped fiber laser. With this photometer, absolute accuracy of reflection and transmission measurements was about ±0.1% and, therefore, losses were calculated with precision of 10^{-3} cm^{-1}. Spectra measured using Perkin Elmer Lambda 950 were stitched to the precise photometric data at 1085 nm. Using this technique, the absolute precision of the whole spectrum was improved to 10^{-3} cm^{-1}.

2.4. Measurements of induced absorption and scattering

The thermal development process of UV-exposed PTR glass relies on the appearance of silver containing particles that participate in the nucleation process followed by the growth of sodium fluoride crystals which cause the appearance of a permanent refractive index change [7,8]. It is well-known that the appearance of silver colloidal particles induces a plasmon resonance that results in an induced absorption band whose position and width depend on their composition and diameter. In Ref. [16], it was shown that depending on the size distribution and on the presence of halides (bromine or chlorine for example), the position of the induced absorption band may vary from 400 to 600 nm. Typical losses spectrum of UV-exposed (4 J/cm^2 at 325 nm) and thermally developed (1 h at 515 °C) PTR glass in the range from 300 to 1500 nm is shown in Fig. 1. Several sources contribute to the losses of UV exposed and thermally developed PTR glass. In UV region, there is the superposition of the absorption of the original glass, mainly a combination of Ce^{3+} and Ce^{4+} absorption bands [17], the induced absorption of silver containing particles and color centers [10], and scattering. In the visible and near-IR ranges, the main contributions are from induced absorption of silver containing particles and scattering. Multiple, overlapped induced absorption bands combined with scattering complicate the analysis of such spectra. However, it was shown [18,19], that induced absorption of silver containing particles can be completely bleached by the second harmonic of a Nd:YAG laser at 532 nm. Therefore, using this technique it is possible to extract the induced absorption spectrum by subtracting the losses spectra before and after this optical bleaching. Fig. 2 shows the typical induced absorption spectrum of UV exposed and thermally developed PTR glass. One can see that this spectrum has a maximum near 465 nm (22,000 cm^{-1}) and extends from 300 to 1500 nm.

It was found that additional scattering in PTR glass could not be detected after UV-exposure and after nucleation at low temperatures but it appears only after thermal development when a crystalline phase of NaF precipitated. To extract the spectral dependence of scattering, the absorption spectrum of virgin PTR glass was subtracted from a loss spectrum of the same PTR glass sample that underwent UV exposure, thermal development and optical bleaching described in the previous paragraph. This spectrum is shown in Fig. 3. It includes scattering and changes of
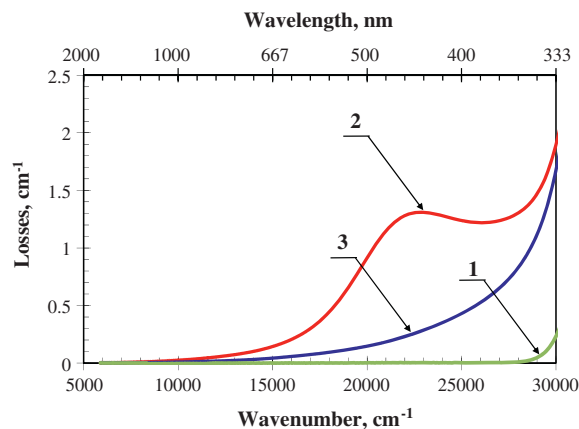

Fig. 1. Spectra of total internal loss in a PTR glass sample. (1) Original absorption spectrum, (2) after exposure to UV radiation at 325 nm for 4 J/cm^2 and development for 1 h at 515 °C, (3) after additional bleaching by visible radiation at 532 nm.
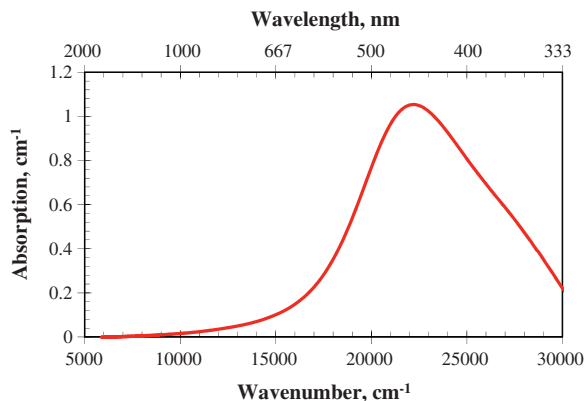
Fig. 2. Absorption induced in PTR glass by UV-exposure and thermal development subsequently bleached by visible radiation (difference between curves 2 and 3 in Fig. 1).
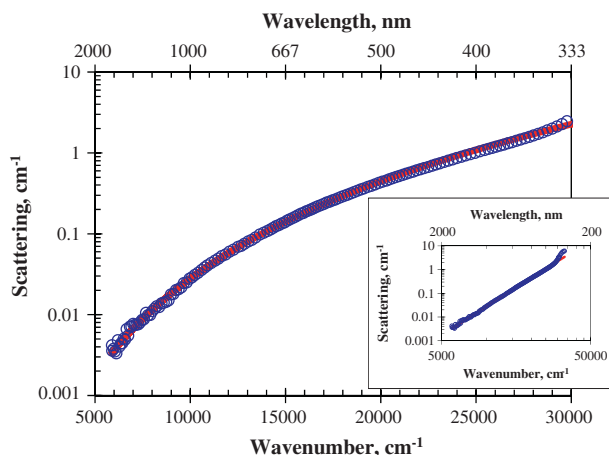

Fig. 3. Scattering induced in PTR glass by UV exposure and thermal development (difference between curves 3 and 1 in Fig. 1 – blue circles) and theoretical spectrum of scattering according to Eq. (4) (red curve). Vertical axis is in logarithmic scale and the small inserted graph shows the same data when both axes are displayed on logarithmic scales. (For interpretation of the references to colour in this figure legend, the reader is referred to the web version of this article.)

absorption that could not be bleached, e.g. absorption of different forms of cerium resulted from its photoionization. It will be shown later that the contribution of absorption in this spectrum is negligible in all parts except the narrow region close to 300 nm.

3. Results

3.1. Analysis of the induced absorption in PTR glass

3.1.1. Gaussian decomposition of induced absorption spectra

As discussed in Section 2.4, the induced absorption spectrum is very broad and potentially complex. A common way to perform the analysis of complex absorption bands consists in using a linear combination of bands with Gaussian profiles in wavenumber (or energy) space [20,21]. Using this technique, it is possible to model the experimental induced absorption spectrum ($A_{exp}(\sigma)$), where sigma is the wavenumber, by a theoretical spectrum ($A_{th}(\sigma)$) equal to:

$$A_{th}(\sigma) = \sum_{i=1}^{4} G_i(\sigma) = \sum_{i=1}^{4} G_i^0 \exp\left\{-\frac{(\sigma - \sigma_i^0)^2}{2\Delta\sigma_i^2}\right\} \quad (1)$$

where $G_i(\sigma)$ is the Gaussian function, G_i^0, its amplitude, σ_i^0, the position of its maximum and $\Delta\sigma_i$ its half width at $1/e^2$. Fitting is performed by minimizing the deviation of the model to the experimental curve. To achieve this, a figure of merit, defined as the sum of the quadratic errors between model and experimental data for each wavenumber, is calculated for each set of parameters and an optimal set of parameters are determined by minimization of this figure of merit:

$$\left[G_i^0, \sigma_i^0, \Delta\sigma_i\right] = \min_{G_i^0, \sigma_i^0, \Delta\sigma_i} \left\{\int_{\sigma_{min}}^{\sigma_{max}} [A_{exp}(\sigma) - A_{th}(\sigma)]^2 \, d\sigma\right\} \quad (2)$$

Position and width of each Gaussian function is fixed and is thus the same for each spectrum that is modeled. The number of Gaussian functions is determined as the lowest number that allows fitting of spectra with precision better or equal to the precision of the measurement, i.e. within a few percent. It was found that for induced absorption spectrum in PTR glass, four Gaussian bands are required to perform a fit with RMS < 5% for all the experimental data obtained in short wavelength range ($\lambda < 550$ nm but larger than 335 nm) for different dosages and conditions of thermal development (e.g. Fig. 2 showing the induced absorption spectrum of a PTR glass exposed with 4 J/cm² and thermally developed for 1 h @ 515 °C). Parameters of these bands are summarized in Table 1. However, it was found that the usage of Gaussian functions is not enough to model the absorption spectra in long wavelength range ($\lambda > 550$ nm). To provide a reasonably small RMS, it was necessary to introduce a new function to properly account for the slow absorption decrease in the long wavelength part of the induced absorption spectra.

3.1.2. Urbach tail in long wavelengths range of induced absorption spectrum

It was shown for silver halide crystals that the long wavelength shoulders of exciton absorption bands are described by exponential functions and not by Gaussian ones [22]. Later this so called Urbach rule was found for extrinsic [23], intrinsic [24] and induced [25] absorption spectra in silicate glasses. To overcome the problem of fitting the long wavelength tail of induced absorption spectrum in PTR glass, which can be associated with silver and bromine containing particles, the Urbach rule was applied [22]. Based on this model, the long wavelengths tail of the G_1 and G_2 Gaussian functions can be replaced with an exponential function defined as:

$$E_i(\sigma) = E_i^1 \exp\left(\alpha_i \frac{\sigma}{\sigma_i^1}\right) \quad (3)$$

where E_i^1 and α_i are two constants and σ_i^1 is the wavenumber of stitching between the Gaussian and the exponential functions. Introducing exponential tails for both long wavelength Gaussian bands G_1 and G_2, associated with silver halide particles, allows fitting the induced absorption spectrum in PTR glass with RMS < 5%. The parameters used for each exponential band are shown in Table 2. The best fitting was found for the same slopes of exponential tails (α_i/σ_i^1 ratio) for both absorption bands. Fig. 4 shows how these two bands allow a good fit between model and data over a wide range of wavelength/wavenumber (from 350 nm (30,000 cm⁻¹) up to 1500 nm (7000 cm⁻¹)).

Table 1
Parameters of the Gaussian bands used for the fitting the induced absorption spectrum.

	G_4	G_3	G_2	G_1
σ_i^0 (cm⁻¹)	26,575	24,275	22,000	19,500
$\Delta\sigma_i$ (cm⁻¹)	3465	2055	3200	2800
λ_i^0 (nm)	376	412	455	513

Table 2
Parameters of the exponential tails used for the fitting of silver containing particles absorption band.

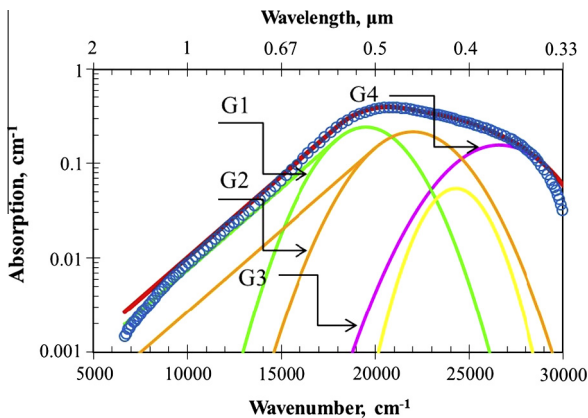|	E2	E1
α_i	8	7.2
σ_i^1 (cm^{-1})	20,000	18,000
α_i/σ_i^1 (cm)	4.E−04	4.E−04

Fig. 4. Decomposition of the induced absorption spectrum in PTR glass using Gaussian and exponential functions. G_1 and E_1 are in green, G_2 and E_2 in orange, G_3 in yellow and G_4 in pink. Experimental data are blue circles while the model prediction is in red. (For interpretation of the references to colour in this figure legend, the reader is referred to the web version of this article.)

3.1.3. Nucleation

It was demonstrated in Ref. [10], that when PTR glass is aged at 480 °C, silver containing nuclei appear while little to no NaF crystal growth can be observed. It was demonstrated that the induced absorption appears concurrently with silver containing nuclei and its spectral shape evolves during heat treatment. This induced absorption was simply associated with silver bromide particles [10]. Using the model presented in the two previous sections, the evolution of the induced absorption spectrum was revisited. PTR glasses were UV-exposed with a dosage of 0.9 J/cm^2 and then nucleated for durations from 5 to 245 min at 480 °C. Absorption spectra were measured after each thermal treatment and induced absorption spectra were retrieved from experimental data (Fig. 5). One can see that induced absorption arises during first few minutes and its intensity is weakly dependent on aging time. However, the spectral shape of induced absorption evolves during the heat treatment process. The maximum of absorption spectrum
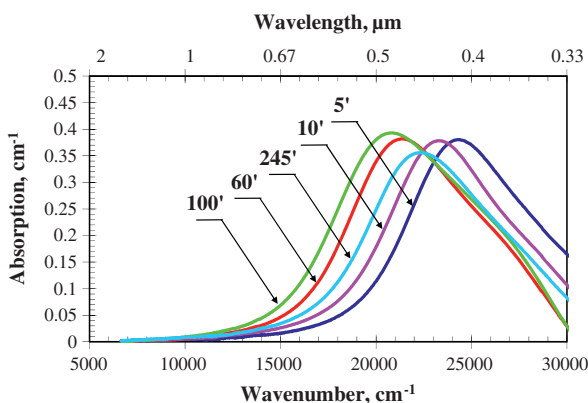
shifts to longer wavelengths from 410 to 485 nm, when aging time increases from 5 to 180 min and then shifts back to 465 nm when nucleation duration is further increased. Each induced absorption spectrum was then decomposed using the described earlier sum of four Gaussian and two exponential functions. It was found that the evolution of induced spectrum can be completely described by a combination of the same functions by varying their amplitudes only. The evolution of the amplitude of each band as a function of aging time at 480 °C is shown in Fig. 6. Since the amplitude of the exponential tails is directly related to the amplitude of their corresponding Gaussian bands, only the amplitudes of the Gaussian bands were plotted. Note that the evolution of the components is not monotonic (discussed below).

3.1.4. Crystallization

After analyzing the evolution of the induced absorption spectra during the nucleation process, the evolution of the same bands during crystallization at higher temperatures was studied. UV-exposed PTR glass samples were thermally developed for different durations of 1, 2 and 3 h at 515 °C. The choice of 515 °C comes from the fact that growth occurs much more slowly at 480 °C than at 515 °C and therefore increasing the development temperature permitted us to speed up the processes. Then, the losses spectra were measured and induced absorption spectra were extracted and fitted using the Gaussian and exponential functions described earlier (Tables 1 and 2). Then dependence of the amplitude of each band on thermal treatment duration is plotted in Fig. 7. Similar to the nucleation process, evolution of different absorption bands is not monotonic and it requires a detailed discussion.

3.2. Analysis of the induced scattering in PTR glass

3.2.1. Rayleigh scattering modeling

Scattering in PTR glass appears after precipitation of the microcrystalline phase of NaF. Scattering spectra were retrieved from experimental data as was described in Section 2.4. The spectral dependence of scattering ($S_{th}(\sigma)$) was modeled using a single exponential function:

$$S_{th}(\sigma) = S_0 \left(\frac{\sigma}{\sigma_0} \right)^N \qquad (4)$$

where σ_0 is constant, the scattering coefficient at σ_0 is S_0 (cm^{-1}) and N is a real number. This formula is usually written for wavelengths but we converted it to wavenumbers to have the same units as for Gaussian and exponential fitting of absorption spectra. One can see in the insert of Fig. 3 that the scattering spectrum when plotted in
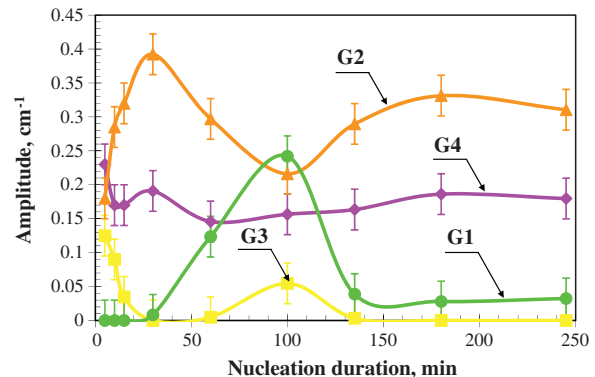

Fig. 5. Induced absorption spectra of PTR glass after UV exposure and nucleation at 480 °C for different times.

Fig. 6. Evolution of the amplitude of the Gaussian components of the induced absorption spectrum in the process of PTR glass nucleation at 480 °C. Error bars are ±0.03 cm^{-1} and were estimated by fitting the experimental data using different initial conditions.
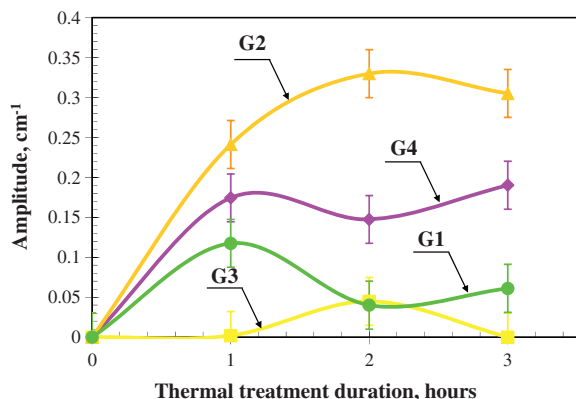
Fig. 7. Evolution of the amplitude of Gaussian components of the induced absorption spectrum in the process of PTR glass development at 515 °C.

Fig. 8. Dependence of scattering (S_0) in PTR glass at 1000 nm on UV-dosage for different thermal treatment durations at 515 °C from 1 to 3 h with $N = 4$ for all.

logarithmic scales is a line with a slope equal to 4, i.e. this spectrum can be fitted by an exponential function Eq. (4) with power N = 4. Actually, the coefficient N determines the type of scattering in a medium. In thermally developed PTR glass, scattering is known to be due to the NaF nano-sized crystals dispersed in the glass matrix and therefore induced scattering follows Rayleigh scattering [8]. The value of power N = 4 confirms Rayleigh scattering in PTR glass. The scattering coefficient S_0 at a fixed wavelength λ_0 (we used $\sigma_0 = 10,000 \ cm-1$, $\lambda_0 = 1 \ \mu m$) was then determined by minimization of the figure of merit at constant N coefficient:

$$S_0 = \min_{S_0}\left\{ \int_{\sigma_{min}}^{\sigma_{max}} [L_{exp}(\sigma) - L_{th}(\sigma)]^2 \, d\sigma \right\} \qquad (5)$$

One can see in Fig. 3 that exponential function describes the scattering spectrum with RMS < 5% in the whole spectral region except the short wavelength region ($\lambda \sim 320$ nm, $\sigma \sim 31,000 \ cm^{-1}$). Deviations of loss spectra in short wavelength region from the exponential function resulted from contribution of absorption of intrinsic and extrinsic color centers that could not be bleached by visible radiation. Extrinsic color centers include different valence states of cerium (and possibly other dopants) resulted from photoionization and trapping of electrons and holes.

3.2.2. Influence of dosage and thermal development duration

In order to study the influence of both the dosage of UV-exposure and the thermal treatment duration, PTR glass samples were UV-exposed with dosages of 0.25, 0.5, 1, 2, 4 and 8 J/cm² and then thermally developed for different durations of 1, 2 and 3 h at 515 °C. Then, loss spectra were obtained after bleaching and subtraction of the original absorption (Fig. 3), and which represent mainly scattering losses, and analyzed. For each of the 18 samples that were prepared and measured, the scattering spectra were fitted with Eq. (4). The dependence of scattering on UV-dosage for the different thermal treatment durations at 515 °C is plotted in Fig. 8. This dependence is dramatically different for different regimes of thermal development. For short duration of thermal development, scattering is the lowest for low dosages, while with increasing the thermal development duration, this tendency is inverted.

4. Discussion

The spectra of induced absorption in PTR glass that could be bleached with pulsed visible radiation have a complex shape with a maximum in the blue/green region. For all studied regimes of UV-exposure and thermal development, these spectra can be accurately decomposed using the sum of 4 Gaussian bands (Table 1). Two of these bands were shown not to be purely Gaussian but to
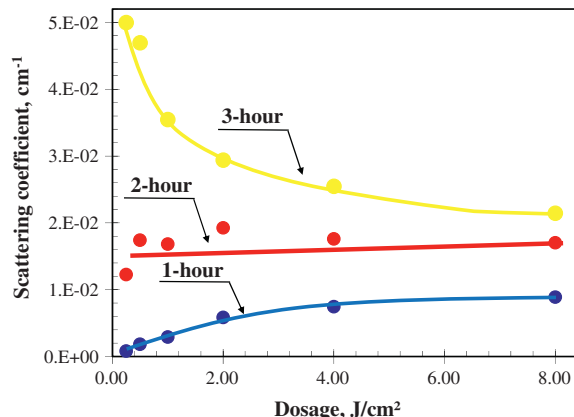
have long wavelength exponential tails (Table 2). This type of decomposition generally assumes that each band can be attributed to one type of particle. Based on the position of each of these bands and some additional hypotheses, each Gaussian band was tentatively associated with a specific type of absorbing center. Regarding the band G_4 with a maximum at ~376 nm, we associated this one with the absorption band of intrinsic hole centers created during UV exposure. This band appears only after UV-exposure and thermal treatment and shows a complex evolution during nucleation and crystallization. A similar absorption band was found in PTR glasses and PTR glass matrix (with no dopants) after γ-irradiation [26] and after exposure to femtosecond radiation [27]. A similar, very well-known band was also observed in the past in several other multi-component glasses [28] and associated with hole centers created during exposure. Thus we can ascribe the G_4 band to atomic scale defects in glass matrix, supposedly to hole color centers.

The second band used in the decomposition model (G_3) is centered at ~412 nm. It is important to recall that the same band (same position and width) was observed in PTR glasses that were not doped with bromine [29], in silver doped glasses and interpreted due to the plasmon resonance of colloidal silver nano-particles formed during the thermal treatment [16,30]. The third band (G_2) with a maximum at 455 nm also was reported several times in the literature. As it appears only in glasses that were doped with bromine and silver, it is therefore legitimate to associate this band with silver bromide particles [31]. The last band (G_1) with maximum at ~513 nm, cannot be associated with any well-known species previously reported in the literature. The experiment with bromine-free PTR glass showed that this band appears only if glass is doped with both bromine and silver proving that this band is associated with some type of silver bromide particles. A similar band with a central wavelength between 500 and 600 nm was observed in PTR-like glass doped with a larger amount of silver [32]. This band was associated with the plasmon resonance of complex nano-particles composed with a AgBr core surrounded by a silver shell, the position of the resonance depending on the ratio between core and shell radii (silver/silver bromide particles).

Using these 4 bands, the evolution of each of the silver containing particles absorption band during the nucleation process was monitored and analyzed (Fig. 5 and 6). The band G_4 of hole centers appears within the first 5 min of the thermal treatment and then its amplitude remains almost constant (within the error of the measurement and uncertainty of fitting). Evolution of the bands G_1 (silver/silver bromide particles), G_2 (silver bromide particles) and G_3 (silver particles) shows strong interconnection. The first particles to appear are silver ones (G_3). After 5 min at 480 °C, the

maximum amplitude of the G_3 band is already reached; its amplitude decreases with further aging and the band disappears after aging for 30 min. This band could not be detected for aging exceeding 30 min, except a sharp peak at 100 min at 480 °C. The origin of this sudden reappearance, whether it is an error of the fitting or a due to some structural transformations, is still unknown. The interesting point is that while the amplitude of the band G_3 of silver particles decreases, the amplitude of the band G_2 of silver bromide particles increases and approaches its maximum when the band of silver G_3 disappears. When the band of silver disappears, the amplitude of the band G_1 starts to increase and the amplitude of the band of silver bromide particles G_2 decreases. When the amplitude of the band G_1 of silver/silver bromide reached its maximum after 100-min aging at 480 °C, the amplitude of the G_2 band of silver bromide particles reaches its minimum. Finally the amplitude of the G_1 band decreases and almost disappears. At that time, the amplitude of the G_2 band increases again until it stabilizes after aging for about 135 min at 480 °C.

This complex interplay between the bands G_1, G_2 and G_3 reflects a series of complex mechanisms of interconversion of silver containing particles. It appears that colloidal silver particles are first created at the initial stage of the nucleation treatment. Then within 30 min at 480 °C, these particles are converted into colloidal silver bromide particles. When all silver bromide colloidal particles have been created, these particles are converted into colloidal silver/silver bromide particles. Maximum absorption, and therefore volume fraction, of these particles is obtained after 100 min at 480 °C. This observation can be compared with the results reported in Ref. [10] where crystallization kinetics were studied by non-isothermal differential scanning calorimetry. In that paper, it was demonstrated that the crystallization peak of UV-exposed PTR glass started to shift to lower temperatures only after 30 min aging at 480 °C. This phenomenon was explained in [10] by creation of nuclei or a catalyzer responsible for the enhancement of crystallization in UV-exposed area of PTR glasses. This correlation between appearance of nucleation centers and an absorption band assigned to silver/silver bromide particles, allows for speculation that silver/silver bromide particles can be associated with those nucleation centers. For thermal treatments exceeding 100 min at 480 °C, the amount of silver/silver bromide particles decreases and the G_2 band of silver bromide increases again as if silver/silver bromide particles were converted back to silver bromide particles. Finally, the structure of the absorption spectrum of silver containing particles tends to stabilize after 135 min at 480 °C. Using this decomposition, some of the very complex mechanisms of heterogeneous nucleation in UV-exposed PTR glass could be revealed. However, as it was reported in Refs. [33,34], the band of silver/silver bromide particles exists only at temperatures below 400 °C and disappears at high temperature. This could be associated with the fact that, at these high temperatures, those particles are expected to melt [16]. This additional observation shows that the role of silver/silver containing particles in the nucleation of UV-exposed PTR glass is even more complex than that in the model described above. However, further investigations are still required to come to a comprehensive description of these processes.

The evolution of the silver containing particles absorption band was also studied during the crystalline phase growth process by aging at 515 °C (Fig. 7). Each of the induced absorption spectra were fitted with the same Gaussian and Gaussian/exponential bands presented in Tables 1 and 2 by optimizing their amplitudes only. Good correspondence of modeled and experimental spectra suggests that the developed model is valid at any moment of the thermal development process while the glass is still transparent. One can see that the magnitude of each band tends to change with time. The first observation is that the G_3 band of silver particles is not detectable after high temperature (515 °C) treatment. The

justification that the small magnitude G_3 band that appears after 2 h of aging (Fig. 7) is a reality but not an artifact of fitting requires some additional study. However, it is possible to suppose that the silver particles are generated early on during the high temperature treatment and are converted to silver bromide particles before they could be detected. The main absorption band of silver bromide particles (G_2) increases in amplitude with aging and comes to saturation. The long wavelength band G_1 shows a non-monotonic behavior at long aging times. Detailed analysis of the absorption spectra after long aging times at high temperature requires some additional effort. First, the longer the thermal development, the higher the scattering (see Fig. 8) that masks induced absorption, especially in the short wavelength region. This effect deteriorates the precision of absorption spectra extraction from the experimental loss spectra. The second possible effect could be connected with the fact that these bands after high temperature treatment might correspond to plasmon but not atomic transitions. Therefore, their width and positions of the bands could depend on the size and chemical structure of each species. It should be repeated that within the precision of the measurements, it was possible to fit all spectra with constant parameters of the bands with the exception of their amplitude. However, more precise measurements might reveal additional details about the evolution of the silver containing particles and their absorption bands.

The last step of this study was the study of the evolution of scattering losses during the thermal treatment of PTR glass. The main supposition is that scattering comes solely from NaF crystals, with refractive index of 1.32 dispersed in the glass matrix having refractive index of 1.5 [7,8]. It was observed that after thermal treatment at 480 °C, for durations from 0 to 240 min, little to no scattering can be detected in the samples. This means that the growth rate of NaF is very slow at these temperatures and that only an undetectable crystal volume fraction was produced after such thermal treatment. The absence of NaF crystals after aging at 480 °C was confirmed by XRD measurements. This result allows for a conclusion that low temperature heat treatment of PTR glass at 480 °C controls the nucleation process while no crystallization occurs within a few hours of aging. The development at temperature of 515 °C results in the appearance of scattering which depends on the dosage of UV-exposure and the thermal treatment duration (Fig. 8) as the NaF crystals grow.

We now analyze the evolution of scattering during the high temperature development at 515 °C that results in growth of nano-crystals of NaF. For small spherical particles ($r \ll \lambda$), scattering can be modeled by Rayleigh scattering and therefore can be expressed with the following approximate formula [35]:

$$S(N_p, r) \propto N_p\, r^6 \tag{6}$$

where N_p is the volume fraction of crystalline phase, r is the radius of crystals. Using this formula, the dependence of scattering on dosage of UV-exposure for different thermal treatment duration at 515 °C can be analyzed. According to Fig. 8, after aging for 1 h at 515 °C, scattering grows with a dosage increase. This means that for a short period of thermal development, crystals do not have enough time to grow, volume fraction of crystals is far from saturation, no depletion of sodium and fluorine occurs, and therefore crystal radius (r) is about the same for any dosage. However, the concentration of nucleation centers and therefore NaF crystals number density and volume fraction (N_p) is increased in the area exposed with higher dosage. According to Eq. (6), an increase of volume fraction causes the increase of scattering at higher dosages.

Comparing to a short development time, aging for 3 h at 515 °C results in higher scattering and an opposite dependence of scattering on dosage where scattering decreases with increasing dosage (Fig. 8, curve 3). This effect is associated with the fact that there

are two competing effects, i.e. the effects of crystal size and crystal number density that have different amplitudes of contribution. Actually, for longer thermal developments, crystals have time to grow, depletion of sodium and fluorine occurs, the volume fraction of crystalline phase (N_p) approaches saturation and has a weak dependence on dosage. Therefore regions where the concentration of nucleation centers is low (low dosage area) enable the growth of a small number of large crystals, while regions where nucleation centers concentration is high (high dosage area) have a great number of small crystals. Due to the 6th power dependence of the scattering versus crystal radius, scattering decreases with dosage because of decreased size of individual crystals. Thermal development for 2 h at 515 °C shows almost no dependence of scattering on dosage (Fig. 8, curve 2) which means that these effects compensate for one another.

Often, the concentration of crystals in two-phase systems is estimated by magnitude of scattering resulted from difference on refractive indices in crystalline and vitreous phases. However, effect of crystallite size on intensity of scattering is higher than volume fraction of crystalline phase. For example, it is known that induced refractive index in PTR glass is the result of precipitation of nano-sized crystalline phase of NaF and that the magnitude of the refractive index change is proportional to the magnitude of X-ray diffraction [7,8]. While scattering is the result of the precipitation of the same crystals, there is no simple correlation between intensities of scattering and photo-induced refractive index change (difference of the average refractive indices in UV-exposed and unexposed regions). Depending on the required refractive index change, the use of low or high dosage in combination with different schedules of thermal development allows optimizing the losses of holographic optical elements.

5. Conclusions

The experimental study and modeling of induced absorption and scattering spectra in photo-thermo-refractive glasses exposed to UV-radiation and aged at elevated temperature have shown that, under all studied conditions of exposure and thermal treatment, induced absorption spectra can be described by a combination of four Gaussian bands (two of them with Urbach exponential tails) and scattering by a single exponential function with power of 4 consistent with classical Rayleigh scattering. These four bands were associated with intrinsic hole centers, and three types of particles consisting of silver, silver bromide and silver bromide with silver shelf (silver/silver bromide). At the initial stage of thermal development at low temperatures, silver particles appear in the beginning then convert to silver bromide containing ones. The longest wavelength band of silver/silver bromide with a maximum at 513 nm was associated with nuclei or catalyzers of the nucleation process. The second stage of thermal development at higher temperatures results in the gradual growth of absorption of both silver bromide and silver/silver bromide absorption bands. Rayleigh scattering in UV-exposed PTR glasses aged at higher temperatures is caused by nano-crystals of NaF. For short development times, scattering increases with dosage because of increased volume fraction of crystalline phase. For long development times, scattering decreases with dosage because of decreased size of individual crystals.

Acknowledgment

References

[1] L.B. Glebov, Volume hologram recording in inorganic glasses, Glass Sci. Technol. 75 C1 (2002) 73–90.
[2] L.B. Glebov, Photochromic and photo-thermo-refractive (PTR) glasses, in: Encyclopedia of Smart Materials, John Wiley & Sons, New York, 2002.
[3] Oleg M. Efimov, Leonid B. Glebov, Vadim I. Smirnov, High efficiency volume diffractive elements in photo-thermo-refractive glass, Patent No. US 6,673,497 B2, January 6, 2004.
[4] O. Andrusyak, V. Smirnov, G. Venus, G. Rotar, L. Glebov, Spectral combining and coherent coupling of lasers by volume Bragg gratings, IEEE J. Sel. Top. Quant. Electron. 15 (2009) 344–353.
[5] L.B. Glebov, Volume holographic elements in a photo-thermo-refractive glass, J. Holography Speckle 5 (2008) 1–8.
[6] W. Höland, G. Beall, Glass–Ceramic Technology, American Ceramic Society, Westerville, Ohio, 2002.
[7] T. Cardinal, O.M. Efimov, H.G. Francois-Saint-Cyr, L.B. Glebov, L.N. Glebova, V.I. Smirnov, J. Non-Cryst. Solids 325 (2003) 275–281.
[8] K. Chamma, J. Lumeau, L. Glebova , L.B. Glebov, Effect of dosage and thermal treatment on photo-thermo-refractive glass crystallization properties, International Congress on Glass (Salvador, Brazil), paper 326, September 2010.
[9] L. Glebova, M. Klimov, K. Chamma, L.B. Glebov, Photo-Structural Transformations in photo-thermo-refractive glass, in: International Congress on Glass, Prague July 1–5, 2013.
[10] J. Lumeau, A. Sinitskiy, L.N. Glebova, L.B. Glebov, E.D. Zanotto, Spontaneous and photo-induced crystallization of PTR glass, Phys. Chem. Glasses: Eur. J. Glass Sci. Technol. B 48 (4) (2007) 281–284.
[11] O.M. Efimov, L.B. Glebov, L.N. Glebova, K.C. Richardson, V.I. Smirnov, Appl. Opt. 38 (1999) 619.
[12] O.M. Efimov, L.B. Glebov, S. Papernov, A.W. Schmid, in: Laser-Induced Damage in Optical Materials, Proc. SPIE 3578 (1999) 554.
[13] O.M. Efimov, L.B. Glebov, V.I. Smirnov, Opt. Lett. 23 (2000) 1693.
[14] J. Lumeau, A. Sinitskiy, L.N. Glebova, L.B. Glebov, E.D. Zanotto, Method to assess the homogeneity of photosensitive glasses: application to photo-thermo-refractive glass, J. Non-Cryst. Solids 355 (2009) 1760–1768.
[15] O.M. Efimov, L.B. Glebov, H.P. Andre, Measurement of the induced refractive index in a photothermorefractive glass by a liquid-cell shearing interferometer, Appl. Opt. 41 (2002) 1864–1871.
[16] A.V. Dotsenko, L.B. Glebov, V.A. Tsekhomsky, Physics and Chemistry Of Photochromic Glasses, CRC Press, 1998.
[17] M. Anne, J. Lumeau, L. Glebova, L.B. Glebov, Specific absorption spectra of cerium in multicomponent silicate glasses, J. Non Cryst. Solids 356 (44–49) (2010) 2337–2343.
[18] L.B. Glebov, V.I. Smirnov, Interaction of photo-thermo-refractive glass with nanosecond pulses at 532 nm, Laser-induced damage in optical materials, Proc. SPIE 5273 (2004) 396–401.
[19] J. Lumeau and L. B. Glebov, Mechanisms of optical bleaching of silver containing particles in photo-thermo-refractive glass, in: International Congress on Glass (Salvador, Brazil), paper 320, September 2010.
[20] L.B. Glebov, E.N. Boulos, Absorption of iron and water in the Na₂O–CaO–MgO–SiO₂ glasses II: selection of intrinsic, ferric, and ferrous spectra in the visible and UV regions, J. Non-Cryst. Solids 242 (1998) 49–62.
[21] P. Pelikán, M. Čeppan, M. Liška, Applications Of Numerical Methods In Molecular Spectroscopy, CRC Press, 1994.
[22] F. Moser, F. Urbach, Optical absorption of pure silver halides, Phys. Rev. 102 (6) (1956) 1519–1523.
[23] F.N. Steele, R.W. Douglas, Phys. Chem. Glasses 5 (1965) 246.
[24] L.B. Glebov, L.B. Popova, M.N. Tolstoi, On the fundamental absorption spectrum in simple silicate glasses, Sov. J. Opt. Technol. 42 (1975) 214–216.
[25] L.B. Glebov, Radiation coloring in the 600–1000 nm region of high purity sodium calcium silicate glass, Sov. J. Glass Phys. Chem. 9 (1983) 242–244.
[26] L. Glebov, L. Glebova, E. Rotari, A. Gusarov, F. Berghmans, Radiation-induced absorption in a photo-thermo-refractive glass Photonics for Space Environments X, in: E.W. Taylor (Ed.), Proc. SPIE 5897 (2005). 58970J-1–58970J-6.
[27] L. Siiman, J. Lumeau, L.B. Glebov, Nonlinear photosensitivity of photo-thermo-refractive glass by high intensity laser irradiation, J. Non Cryst. Solids 354 (2008) 4070–4074.
[28] J. Schulman, W. Compton, Color Centers in Solids, Pergamon Press, 1963.
[29] L. Glebova, J. Lumeau, M. Klimov, E.D. Zanotto, L.B. Glebov, Role of bromine on the thermal and optical properties of photo-thermo-refractive glass, J. Non-Cryst. Solids 354 (2008) 456–461.
[30] K.J. Berg, P. Grau, D. Nowak-Wozny, M. Petzold, M. Suszynska, On the sensitivity of optical and mechanical characteristics of the Na+ Ag+ exchange process in soda-lime silicate glass, Mater. Chem. Phys. 40 (2) (1995) 131–135.
[31] Product data sheet on silver bromide. (www.photonic.saint-gobain.com).
[32] A.P. Nacharov, N.V. Nikonorov, A.I. Sidorov, V.A. Tsekhomskii, Influence of ultraviolet irradiation and heat treatment on the morphology of silver nanoparticles in photothermorefractive glasses, Glass Phys. Chem. 34 (6) (2008) 693–699.
[33] J. Lumeau, L. Glebova, G.P. Souza, E.D. Zanotto, L.B. Glebov, Effect of cooling on the optical properties and crystallization of UV-exposed photo-thermo-refractive glass, J. Non-Cryst. Solids 354 (2008) 4730–4736.
[34] J. Lumeau, L. Glebova, L.B. Glebov, Evolution of absorption spectra in the process of nucleation in photo-thermo-refractive Glass, Adv. Mater. Res. 39–40 (2008) 395–398.
[35] H. Masuda, K. Higashitani, H. Yoshida, Powder Technology Handbook, third ed., CRC Press, 2006.